Magnetoreflection studies of tin-doped bismuth

A. Misu*

*Department of Physics, Faculty of Science, University of Tokyo, Tokyo 113, Japan
and Center for Materials Science and Engineering, Massachusetts Institute of Technology,
Cambridge, Massachusetts 02139*

T. C. Chieu* and M. S. Dresselhaus

*Department of Electrical Engineering and Computer Science and Center for Materials Science
and Engineering, Massachusetts Institute of Technology, Cambridge, Massachusetts 02139*

J. Heremans*

*Laboratoire de Physico—Chimie et de Physique de l'État Solide, Place Croix du Sud, 1,
B-1348 Louvain-La-Neuve, Belgium
and Center for Materials Science and Engineering, Massachusetts Institute of Technology,
Cambridge, Massachusetts 02139*

(Received 7 December 1981)

The validity of the rigid-band model for bismuth is generally confirmed by magnetoreflection experiments on tin-doped samples in which the Fermi energy has been lowered by ~ 50 meV. Detailed analysis of the measurements, however, shows a significant relative increase in the small L-point band gap due to tin doping. The introduction of charged impurities also gives rise to Landau-level transitions which are forbidden in pure bismuth. Two resonance lines are found, neither of which can be associated with transitions between the Landau levels of the rigid-band scheme. Possible assignments of these lines are discussed.

I. INTRODUCTION

This work is the first direct study of the effect of doping on the electronic structure of the semimetal bismuth. Previous work has focused on the effect of doping on the Fermi surfaces and these results were interpreted in terms of a rigid-band model.[1-9] The rigid-band model assumes that the electronic energy-band structure remains quantitatively unchanged by the doping.

The present study is directed toward an investigation of the validity of the rigid-band approximation for the case of tin-doped bismuth. We show here using the magnetoreflection technique that the rigid-band approach is approximately valid, though notable departures occur with regard to the behavior near the small L-point band gap and the selection rules governing Landau-level transitions.

In the doping experiments on bismuth, elements from column IV or column VI of the Periodic Table have been added either to lower or raise the Fermi level.[1-9] Because of the low intrinsic carrier concentration of bismuth ($\sim 3 \times 10^{17}$ cm^{-3} at ~ 4 K), impurity concentrations as low as 10^{18} cm^{-3} have a major effect on the Fermi level and

on the Fermi surface. This behavior is in contrast to the addition of isoelectronic impurities such as antimony into bismuth, where large quantities (several percent) of antimony must be added in order to significantly affect the electronic properties.[10-12] For these isoelectronic impurities the form of the electronic structure remains essentially unchanged, but the band parameters governing the dispersion relations are modified because of such factors as differences in the spin-orbit coupling constants.

Because the impurity concentrations necessary to move the Fermi level significantly are small,[5-9] the perturbation to the electronic dispersion relations is expected to be small. The magnetoreflection experiment is, however, sufficiently sensitive to measure such small differences, as is demonstrated in the present work.

II. BACKGROUND

The addition of the group-IV element tin to the group-V semimetal bismuth has long been known[2-4] to lower the Fermi level. Noothoven

van Goor[5] established that tin is a monovalent ac-
ceptor in bismuth by comparing the density of ex-
cess holes (as measured by the Hall effect at 4.2 K)
to the density of extrinsic tin atoms actually
present in the crystal (as measured by a radioactive
tracer technique). The Shubnikov—de Haas (SdH)
effect has been used extensively to study the band
structure of both tin-[6,7] and tellurium-[9] doped
bismuth. For the tin-doped samples with concen-
trations up to 0.1 at. % tin, corresponding to an
excess hole concentration of roughly 2×10^{19} cm^{-3},
the major effect of tin doping is the lowering of
the Fermi level with respect to the various band
edges in pure bismuth. Using this criterion it is
sufficient to measure the low-temperature Hall
coefficient of a tin-doped bismuth sample to obtain
the density of carriers and, using the density of
states of pure bismuth,[13] to obtain a good estimate
for the location of the Fermi energy.

The addition of tin to bismuth increases the size
of the T-point hole pocket and decreases the size
of the L-point electron pockets until a tin concen-
tration of 1.7×10^{18} cm^{-3} is reached, where the
Fermi level falls below the L-point conduction-
band minimum and only the T-point holes contri-
bute to the transport properties. With the further
addition of tin the T-point hole concentration con-
tinues to increase until a concentration of 2.7
$\times 10^{18}$ cm^{-3} is reached, where the Fermi level falls
below the L-point valence-band maximum and
holes begin to appear. At a concentration of
5×10^{18} cm^{-3} the density of the L-point holes is
equal to that of the L-point electrons in pure
bismuth. A schematic diagram of the variation of
the electron Fermi energy with the excess density
of holes Δ is given in Fig. 1.

The sample used in the present magnetoreflec-
tion study had a density Δ of 4.28×10^{18} cm^{-3} ex-
cess holes as characterized by Hall coefficient mea-
surements at 4.2 K.[14] According to Fig. 1 the Fer-
mi level for this sample is expected to be 16 meV
below the top of the L-point hole or valence band.
Because the Fermi level lies below the L-point
valence-band maximum in our tin-doped bismuth
sample, both the L-point conduction- and valence-
band extrema are unoccupied.

Magnetoreflection studies have been carried out
extensively on pure bismuth,[15−18] including the
temperature[19] and pressure[20] dependence of the
spectra. These studies have contributed in a major
way to establishing the details of the band struc-
ture and Fermi surface near the L point of the
Brillouin zone. The conduction- and valence-band

extrema lie very close to each other and are well
separated from the other bands at the L point.
The two bands (the symmetric L_s conduction band
and the antisymmetric L_a valence band) are of dif-
ferent parity and interact with each other strongly
through the $\vec{k} \cdot \vec{p}$ interaction.[21]

In a magnetic field Landau levels are formed in
both conduction and valence bands. Because of
the large spin-orbit coupling in bismuth the energy
levels are conventionally[21,22] labeled by the quan-
tum number j rather than the Landau-level quan-
tum number n where

$$j = n + \tfrac{1}{2} - s , \tag{1}$$

and $s = \pm \tfrac{1}{2}$ is the spin. The energy of the $j \neq 0$
magnetic levels in the conduction band with
respect to the center of the band gap is written as:

$$E^c_{j \neq 0, s}(k_H = 0) = (\epsilon^2 + j\gamma H)^{1/2} - 2\alpha s H , \tag{2}$$

where $\hbar k_H$ is the crystal momentum along the
magnetic field H and ϵ is half of the gap energy
E_G,

$$\epsilon = E_G / 2 . \tag{3}$$

The field coefficient γ is directly related to the
momentum matrix element between the two bands
$\langle c \mid p \mid v \rangle$,[23]

$$\gamma = E_G \beta^* = \frac{e\hbar}{2m^2 c} \langle c \mid p \mid v \rangle \langle v \mid p \mid c \rangle , \tag{4}$$

and can also be expressed in terms of the effective
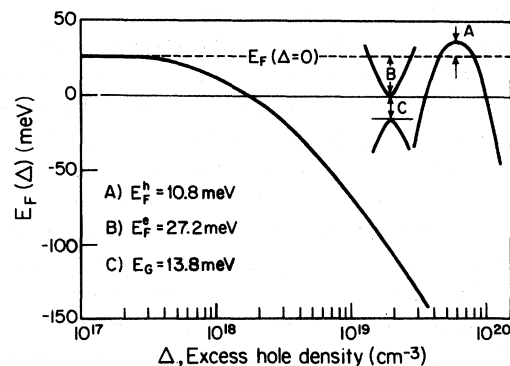Bohr magneton β^*. In Eq. (4) m is the free-

FIG. 1. Variation of the Fermi energy E_F with excess
density of holes Δ in acceptor-doped bismuth, with the
zero of energy taken at the L-point conduction-band
minimum. The figure shows the Fermi energy for the
L-point electrons, T-point holes, and the L-point band
gap of pure bismuth (Refs. 18,24,25,26).

electron mass. The splitting factor α results from the $\vec{k} \cdot \vec{p}$ perturbation contribution from the bands not included explicitly in the two-band model and is assumed to be the same for all $j \neq 0$ levels.[18] The factor α is written as the product of the effective g factor G and the effective Bohr magneton β^*,

$$\alpha = G\beta^* . \tag{5}$$

Since α is small the pairs of energy levels $E(n, -\frac{1}{2})$ and $E(n+1, +\frac{1}{2})$, which have the same quantum number j, are nearly degenerate.

The energy of the $j = 0$ conduction level, which is not degenerate within the conduction band, lies very near to the nondegenerate $j = 0$ level of the valence band. Taking into account the interaction between the two $j = 0$ levels, the conduction-band-level energies at $k_H = 0$ are given by[16−18,23]:

$$E^c_{j=0,s=1/2}(k_H = 0) = [(\epsilon - \alpha'H)^2 + (\delta H)^2]^{1/2} , \tag{6}$$

where α' and δ are related to the effective g factor G_0 and the coupling parameter P by:

$$\alpha' \equiv |G_0\beta^*| \tag{7}$$

and

$$\delta \equiv P\beta^* . \tag{8}$$

The Landau levels in the valence band are the mirror images of those in the conduction band,

$$E^v_{j,s} = -E^c_{j,s} . \tag{9}$$

These approximations called the modified two-band model[16,18,21,23] were shown to be sufficiently precise for interpreting magnetoreflection results,[15−20] as well as SdH and de Haas−van Alphen (dHvA) measurements of the Fermi surface.[24] The magnetic energy levels are shown schematically in Fig. 2.

The optical transition from a $j \neq 0$ level in the valence band to a $j' \neq 0$ level in the conduction band peaks at the critical point $(k_H = 0)$ in the joint density of states for the transition and obeys the spin-selection rule,

$$\Delta s = \pm 1 , \tag{10}$$

because the spin s in the valence band corresponds to that of a hole. In the case of the $1 \leftrightarrow 2$ transitions, the four transitions shown on the left side of Fig. 2 are not resolved and thus contribute to the same resonance line, because the splitting factors α are almost the same for both the $j = 1$ and $j' = 2$ levels, and because the level energies are symmetric
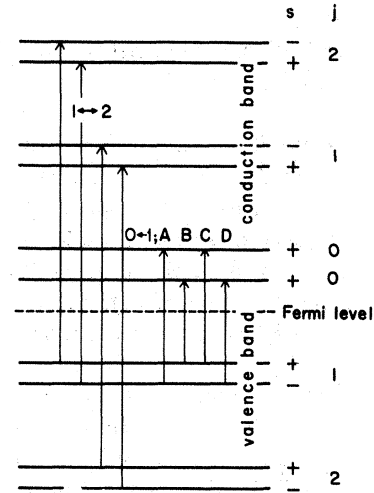

FIG. 2. Magnetic level scheme near the L point of bismuth in the presence of a magnetic field. The levels are labeled by the quantum number j and the spin s, where $+$ and $-$ denote, respectively, $s = +\frac{1}{2}$ and $s = -\frac{1}{2}$. Arrows represent optical transitions. On the left side two $\Delta s = \pm 1$ pairs of transitions, $(j)_{\text{valence}} \rightarrow (j+1)_{\text{conduction}}$ and $(j)_{\text{conduction}} \leftarrow (j+1)_{\text{valence}}$, contribute to the same resonance in pure bismuth. On the right side, the A, B, C, and D transitions are shown for the case of the $0 \leftarrow 1$ transitions. For the tin-doped bismuth sample with $\Delta = 4.28 \times 10^{18}$ cm^{-3} excess holes, the Fermi level is expected to lie between the $j = 0$ and $j = 1$ levels in the valence band at all magnetic fields used in the present experiment.

with respect to the center of the energy gap.

In pure bismuth the $j \leftrightarrow j + 1$ transitions occur subject to the selection rule

$$\Delta j = \pm 1 , \tag{11}$$

which includes the spin-selection rule given by Eq. (10) and the orbital-selection rule, $\Delta n = 0$ and $\Delta n = \pm 2$, which is a practical approximation of the even-integer selection rule $\Delta n = \pm 2l$, applicable to nonparabolic bands.

The transitions between the $j = 1$ and $j' = 0$ levels, denoted as the $0 \leftarrow 1$; A, B, C, and D transitions in Fig. 2, are qualitatively different from the $j \neq 0$ to $j' \neq 0$ transitions discussed above.[18] The A and C transitions are both interband transitions, where A is the spin-conserving and C is the spin-flipping transition. The B and D transitions are, respectively, the cyclotron resonance and the spin-flipping intraband transitions. The joint densities of states for these transitions are different from those for the interband transitions. In pure bismuth for the magnetic field along a binary axis, the Fermi level

lies between the $j = 1$ and $j = 0$ levels in the conduction band for magnetic fields above 13 kG, so that the $0 \rightarrow 1$; A, B, C, and D transitions are observed.[18] Because the Fermi level is expected to lie below the L-point valence-band maximum in the present tin-doped sample, the Landau-level transitions are expected to occur from the $j = 1$ level in the valence band to the two $j = 0$ levels, in contrast to the behavior in pure bismuth; the transitions shown on the right side of Fig. 2 are appropriate to the tin-doped bismuth sample used in the present work.

There are three nonequivalent L points in the Brillouin zone. For a magnetic field applied parallel to a binary axis in crystalline bismuth the L point for which the field H is along one of the principal axes of the hole ellipsoid is the principal L point, while the other two are nonprincipal L points. In the Faraday geometry for this field direction, only transitions between Landau levels associated with the nonprincipal L points are observed in pure bismuth. No magneto-optical resonances for transitions associated with the principal L point and those with the T point are observed because of the heavy cyclotron effective mass for the pertinent cyclotron orbits.[24−27]

III. EXPERIMENTAL DETAILS

The sample used in the present magnetoreflection measurements was grown by Noothoven van Goor, following the Czochralski technique.[5] The long axis of the original sample did not deviate from the bisectrix direction by more than 7°. The original sample was cut into three parts, each of which served for different studies: thermal conductivity and thermopower,[28] electrical conductivity,[29] and temperature dependence of the Hall effect.[13] Because of possible inhomogeneities along the length of the original sample, we estimate that there may be as much as 10% uncertainty in the excess-carrier densities in each of the three parts.[29] The part of the original crystal that was used in the present work was oriented by means of x-rays and a binary face was cut and polished into an optically flat surface.

The magnetoreflection spectra were measured with a setup similar to that used in the previous magnetoreflection experiments on bismuth.[15−19] The sample was mounted on a cold finger of a liquid helium container, with the sample temperature estimated as ∼20 K.[17] The magnetic field

produced by a two-inch-bore Bitter magnet was applied parallel to a binary axis and the maximum attainable field was 147.7 kG.

The infrared light was incident on the binary face of the sample at nearly normal incidence at a reflection angle of about 6°. A Perkin-Elmer monochromator in a single-pass configuration was employed. The spectral purity of the infrared radiation was set to permit a band pass smaller than 0.18 μm, i.e., $(\Delta\lambda/\lambda) < 1.5\%$ for each photon energy used in the experiment.

Changes in the reflected light intensity were observed upon sweeping the magnetic field. The location of the peak intensity was designated as the resonance magnetic field,[16] and we also used the criterion that the resonant fields observed in the up and down sweeps were coincident.

IV. EXPERIMENTAL RESULTS

Shown in Fig. 3 are examples of experimental magnetoreflection traces obtained with the tin-doped bismuth sample. As in the case of pure bismuth the resonant structures appearing in these traces in the lower magnetic field range are qualitatively different from those at high magnetic fields and low photon energies.

In the low-photon-energy and high-magnetic-field regime, up to four intense and broad peaks labeled by $0 \leftarrow 1$; A, B, C, and D in Fig. 3 are observed and are identified with transitions involving the $j = 0$ levels. The reasons for this identification are given in Sec. V. These peaks increase in intensity as they shift to higher magnetic fields with increasing photon energy. The field dependence of these intense and broad peaks can only be followed over a limited photon-energy range since they shift out of our attainable magnetic field range for photon energies above 121 meV.

In the low-magnetic-field range several sharp resonances are observed with resonant fields that increase with increasing photon energy. These resonances are identified with transitions involving predominantly higher Landau levels $j \geq 1$, and are also discussed in Sec. V. At a fixed photon energy as the magnetic field increases, so does the intensity of the resonant structures. As a consequence, the intensity of each resonance of a given type also increases with increasing photon energy, characteristic of Landau-level transitions. The shapes of the resonances labeled $j \leftrightarrow j + 1$ for $j = 1, 2, \ldots$, show a steep rise on the low-magnetic-field side
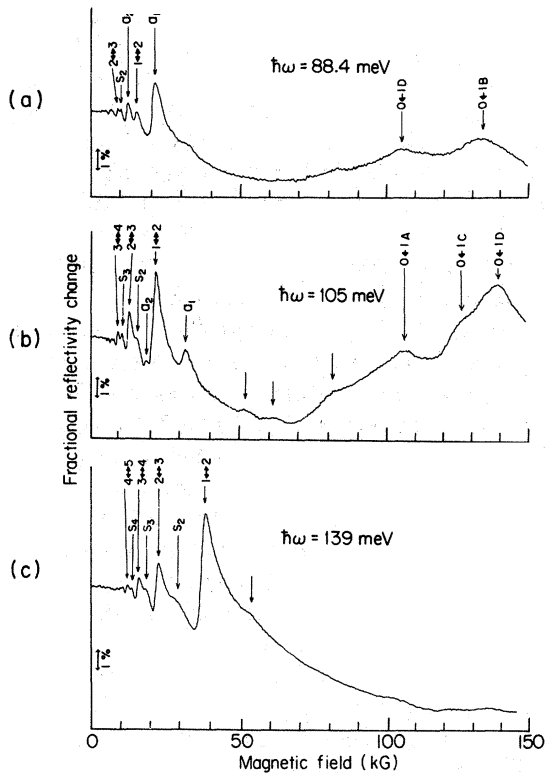
FIG. 3. Experimental magnetoreflection traces for our tin-doped bismuth sample (see text) taken at photon energies (a) $\hbar\omega = 88.4$ meV, (b) $\hbar\omega = 105$ meV, and (c) $\hbar\omega = 139$ meV. The peaks in each trace are classified into four main categories: (1) $0 \leftarrow 1$; A, B, C, and D transitions, (2) the $j \leftrightarrow j + 1$ main series transitions, (3) the s_j satellite components, and (4) the additional a_1 and a_2 structures. Several other very weak structures are also indicated by arrows.

FIG. 4. Fan chart for (1) the $0 \leftarrow 1$; A, B, C, and D transitions, (2) the $j \leftrightarrow j + 1$ main series transitions, (3) the s_j satellite components, and (4) the additional a_1 and a_2 structures in tin-doped bismuth with $\Delta = 4.28 \times 10^{18}$ cm^{-3} excess holes. The dots represent the measured location of the well-defined resonances and the dots in parentheses show the approximate location of a broad and weak structure; these transitions are identified in Fig. 8. The lines connect the measured points of a given line shape.

and a tail toward higher magnetic fields, and are a manifestation of the magnetic field dependence of the joint density of states between the Landau levels of the initial and final states of the transition.[15,16] The general line shape is similar to that of bismuth but the steep initial rise for the doped sample is less sharp, indicative of increased electron scattering due to the increased concentration of charged impurity-scattering centers associated with the tin doping.

The most striking difference between the resonances in Fig. 3 and those in pure bismuth is that every sharp peak appears to be doubled, with a smaller satellite component labeled by s_j at the high-field side of each main resonant $j \leftrightarrow j + 1$ structure. Each satellite component broadens with increasing magnetic field and thus also with increasing photon energy, while the linewidth of each
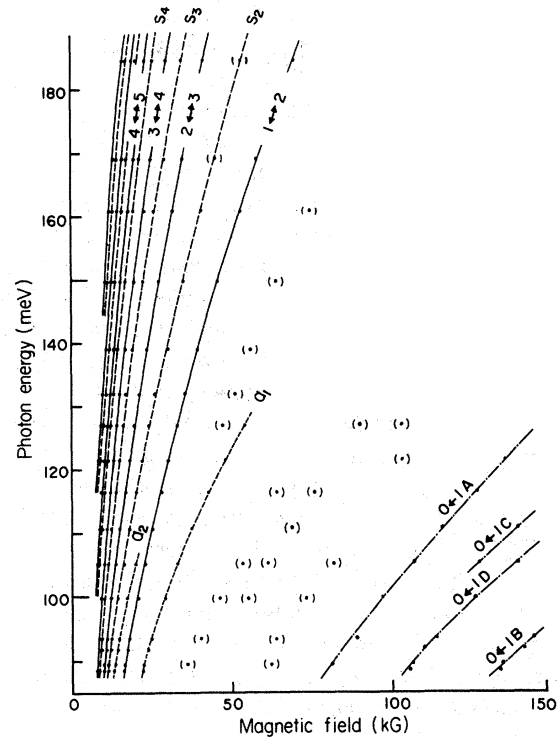
main component has approximately the same dependence on magnetic field and photon energy as in pure bismuth. The relative intensity of the satellite peaks decreases with increasing magnetic field, and for the resonant structure at the highest magnetic field the satellite component is very faint, as is seen in Fig. 3(c) at about 56 kG. This structure can be attributed to the s_1 satellite, but is not labeled in Figs. 3 and 4 because the dependence of this structure on magnetic field and photon energy could not be followed accurately.

In the low-photon-energy and low-magnetic-field range, we observe two additional peaks labeled a_1 and a_2, which are not present in the spectrum for pure bismuth and are not associated with either the main-component or the satellite-component structures discussed above. In Fig. 3(a) for the trace at 88.4 meV, the lowest photon energy of the present

measurements, these additional peaks are the strongest and second strongest peaks in the spectrum. These additional peaks decrease in intensity in comparison with the main resonances as the magnetic field and photon energy are increased and the a_1 and a_2 peaks disappear altogether at about 130 and 110 meV, respectively. The shapes of these additional resonant structures are more symmetric than those for the other resonant structures and exhibit no tails at higher magnetic fields. The a_1 and a_2 structures, furthermore, remain sharp up to the magnetic fields and photon energies where these resonant structures suddenly disappear.

The traces show additional broad structures of very weak intensity. These weak structures are shown by arrows in Fig. 3 but are not labeled. These structures are further discussed in Sec. VII.

The fan chart shown in Fig. 4 summarizes the resonant magnetic fields of each resonant structure discussed above for a number of photon energies. The dots show the locations measured for the well-defined resonances. A dot in parentheses represents the presence of a broad and weak struc-

FIG. 5. Comparison of resonances for the tin-doped bismuth sample ($\Delta = 4.28 \ 10^{18} \ cm^{-3}$ excess holes) with those of pure bismuth. The measured locations are shown with dots and thin solid lines, while the fan chart for Landau-level transitions in pure bismuth is shown by thick solid lines.

ture and shows its approximate location; for these weak structures the errors in the location of the resonance point are as large as ± 5 kG.

The lines which connect the measured points of a given line shape show the relation between the resonant magnetic field and photon energy for: (1) the four $0 \leftarrow 1$; A, B, C, and D peaks, (2) the $j \leftrightarrow j + 1$ resonances, (3) the s_j satellite components, and (4) the a_j additional structures. The dot-dashed curves give the resonant condition of the intense and broad peaks labeled $0 \leftarrow 1$; A, B, C, and D in Fig. 3. These transitions are observed only in the low-photon-energy and high-magnetic-field regime under the present experimental conditions. The solid lines in Fig. 4 correspond to the main series of resonant $j \leftrightarrow j + 1$ structures and the dashed lines correspond to the satellite components s_j. Both the main resonances and the satellite components show similar strong field dependences. These resonances occur with a regular periodicity in the low-magnetic-field range, and are more closely spaced with increasing j. The shorter dashed lines correspond to the additional peaks a_1 and a_2, both of which have a field dependence very similar to, but somewhat smaller than, those of the $j \leftrightarrow j + 1$ main resonant structures and those of the s_j satellite components.

V. ANALYSIS

The identification of the $j \leftrightarrow j + 1$ resonances in the tin-doped bismuth sample mainly comes from a comparison with the fan chart for Landau-level transitions in pure bismuth, where it is found that the main components labeled $j \leftrightarrow j + 1$ lie very near to the allowed $j \leftrightarrow j + 1$ ($j \neq 0$) transitions of pure bismuth. Such a comparison is made in Fig. 5, where the dots are the measured locations of resonant peaks of the tin-doped bismuth sample (the same as those shown in Fig. 4) and the heavy lines are the fan chart for Landau-level transitions in pure bismuth.[17] For example, at a photon energy of 150 meV, the main transition at the highest magnetic field lies at only 1.5 kG below the resonant magnetic field for the $1 \leftrightarrow 2$ transitions of pure bismuth; and below a photon energy of 100 meV this transition is essentially coincident with that in bismuth to within the experimental error. Furthermore, the difference in resonant magnetic field between the main components in the tin-doped bismuth and the $j \leftrightarrow j + 1$ transitions in pure bismuth decreases with increasing quantum number j. From this comparison and a comparison of
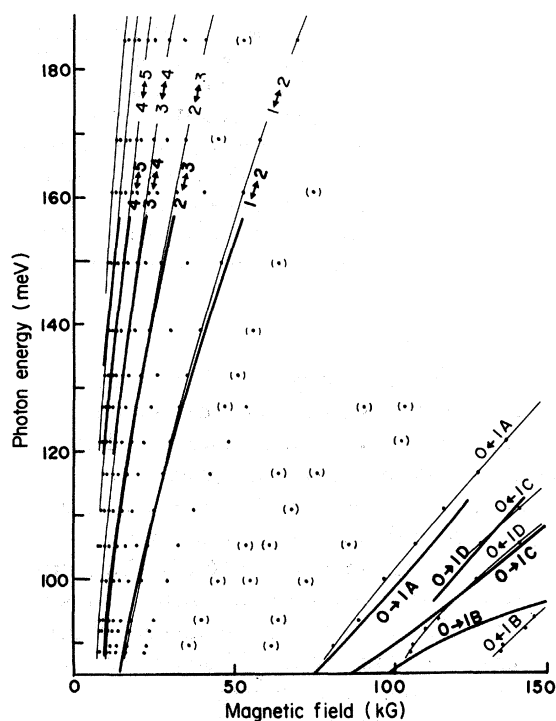
the line shape and the field and photon-energy dependence of the resonant intensity in pure and tin-doped bismuth, the main resonant structures in the tin-doped bismuth sample are identified with the $j \leftrightarrow j+1$ ($j \neq 0$) transitions.

The magnetic field and photon-energy dependences of the intense and broad peaks in the low-photon-energy and high-magnetic-field range also lie near to those of the $0 \rightarrow 1$ transitions denoted by A, D, C, and B in pure bismuth, as are also shown in Fig. 5. Using the same basic model that was applied to the interpretation of these transitions in pure bismuth, the assignments given in Fig. 4 were obtained. Because the Fermi level lies below the L-point valence-band maximum in the present tin-doped sample, as is discussed in Sec. II, the Landau-level transitions occur from the two $j = 1$ valence levels to the two $j = 0$ levels. Thus, in Fig. 4 A and C denote interband transitions from the $j = 1$ level of the valence band, B is the valence-band cyclotron resonance transition, and D is a spin-flipping $0 \leftarrow 1$ Landau-level transition in the valence band. The peaks, rather than some other feature of the structure, are identified with these $0 \leftarrow 1$ transitions. An asymmetric line shape with a tail at lower magnetic fields is found for the structure labeled A, while the peak labeled C appears as a shoulder of the structure labeled D. The sharp-edge structure with a sharp peak, which is observed in pure bismuth[18] in the photon-energy range below about 80 meV, has not been observed in the present study of the tin-doped bismuth sample. The B transition, which is the highest magnetic field component in bismuth, is shifted to higher magnetic fields in the tin-doped sample; the transition A, which is the lowest magnetic field component in bismuth, is shifted to much lower magnetic fields with tin doping; because of the relation between the resonant magnetic field and photon energy for the C and D transitions, as is discussed below, these transitions are found to be interchanged relative to their occurrence in pure bismuth.[18]

From the field dependence of the three $j \leftrightarrow j+1$ ($j = 1,2,3$) transitions, we obtain the field dependence of the energy of each jth level involved in these transitions. The field dependence is obtained on the basis that the energy of the jth level depends on the magnetic field H only through jH, the product of the quantum number and the field. It then follows that when the energy for the $j = 1$ level is found at a field value of H, this is also the energy of the $j = 2$ level at $H/2$, of the $j = 3$ level
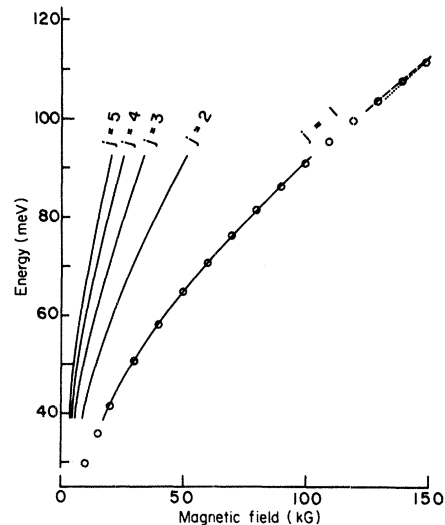

FIG. 6. Magnetic field dependence of the energy of the jth level with respect to the center of the band gap. The solid lines are determined assuming that the energy depends on H only through the product jH. The dashed and dotted lines are the average energies of the A and B transitions and that of the C and D transitions, respectively. The open circles represent the calculated result for E_1^{av} [Eq. (12)], with values $\epsilon = 8.6$ meV and $\gamma = 81.2$ meV^2/kG determined from the least-squares analysis of magnetoreflection spectra in tin-doped bismuth.

at $H/3$, etc. The field dependence of the $j = 2$ level obtained from analysis of the $1 \leftrightarrow 2$ transitions is in good agreement with that obtained from analysis of the $2 \leftrightarrow 3$ transitions. This observation indicates that also for the tin-doped sample the magnetic levels in the valence and conduction bands are mirror images of each other with respect to a common zero of energy. Therefore, the energies of the $j \rightarrow j+1$ and $j \leftarrow j+1$ transitions are the same and both transitions contribute to the same resonance. The results for the field dependence of the levels $1 \leq j \leq 5$ in the conduction band obtained above are shown in Fig. 6, where the energies are measured with respect to a common zero of energy taken as the average energy between each pair of jth levels in the conduction and valence bands.

In the high-magnetic-field portion of Fig. 6 the $j = 1$ level is determined from the average energy between the $0 \leftarrow 1$ transitions labeled A and B and shown by a dashed line, and that between the C and D transitions, shown by a dotted line. These energies are the average between the two components of the $j = 1$ valence level with respect to that of the average between the two $j = 0$ levels.
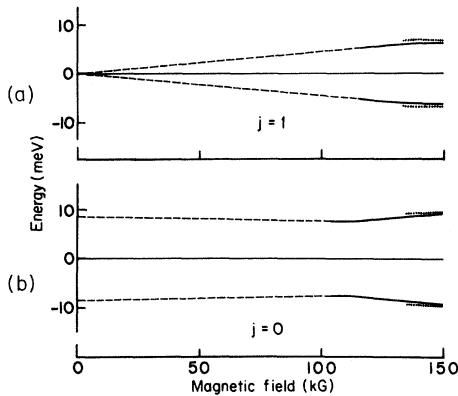
FIG. 7. Magnetic field dependence of the splitting of (a) the $j=1$ level and (b) the $j=0$ level. In each case the energies are shown with respect to their average energies. In (a) the solid and dotted lines are the difference in transition energy between the A and C transitions and that between the D and B transitions, respectively, and the dashed lines are a linear extrapolation to $H=0$. In (b) the solid and dotted lines are the difference in transition energy between the A and D transitions and that between the C and B transitions, respectively, and the dashed lines are a linear extrapolation to $H=0$ so as to coincide with $E_G=17.2$ meV determined by the least-squares analysis.

There is a little difference between the dotted and solid curves but this difference is regarded as an error caused by the uncertainty in reading the peak position of the broad structure of the $0\leftarrow1$ transitions. The lines obtained for the energy of the $j=1$ level from analysis of the $0\leftarrow1$ transition join continuously and smoothly to the results for the $j=1$ level obtained from analysis of the $j\leftrightarrow j+1$ transitions at lower magnetic fields. Accordingly, the average energy of the $j=0$ level (i.e., the center of the L-point band gap) is coincident with the common zero of energy and is thus the average energy between each pair of jth levels in the conduction and valence bands.

To proceed with the analysis the difference in the transition energy between the A and C transitions with respect to their average energy is plotted in Fig. 7(a) with a solid line and that between the D and B transitions with a dotted line. Thus, Fig. 7(a) gives the splitting of the $j=1$ levels relative to their average energy. Correspondingly, in Fig. 7(b) are shown the differences between the A and D transitions (solid line) and between the C and B transitions (dotted line), thereby yielding the field dependence of the $j=0$ valence- and conduction-band levels. In each figure the solid and dotted lines are in good agreement with each other when

the broadening of the transitions is taken into account. From the magneto-optical study alone one cannot distinguish between the upper and lower levels. In Fig. 7(a), however, the splitting of the $j=1$ level tends to zero when the magnetic field decreases to zero; this limit is shown in the figure (dashed line) as a linear extrapolation. The field dependence of this splitting is $\alpha=0.043$ meV/kG, which is found to be almost the same as that for the $j=1$ level in pure bismuth.[18] This agreement is the reason for the present identification of the A, B, C, and D transitions, especially the identification of the second highest and the third highest transitions in energy with the C and D transitions, respectively. Because of this agreement, the splitting shown in Fig. 7(a) is assigned to that of the $j=1$ level, and the initial state for the A and D transitions is assigned to the lower-lying component, while that for the B and C transitions is assigned to the upper-lying component of the $j=1$ level in the valence band.

The splitting of the $j=1$ level is observed as shown in Fig. 7(a). However, no splitting is observed for the $j\leftrightarrow j+1$ transitions, including the $1\leftrightarrow2$ transitions which also involve the $j=1$ level. This situation is the same as that in pure bismuth. It should also be noted here that all the s_j satellite structures are associated with transitions which also exhibit no spin-split components as described in Sec. VII. As is shown in Fig. 6 the energy of the $j=1$ level obtained from the analysis of the $1\leftrightarrow2$ transitions joins continuously to the average energy between the $j=1$ split components determined from analysis of the $0\leftarrow1$ transitions. This observation provides evidence that every $j\neq0$ level has nearly the same splitting factor as that of the $j=1$ level, and that a pair of $\Delta s=\pm1$ transitions contributes to each $j\leftarrow j+1$ and $j\rightarrow j+1$ resonance. For pure bismuth the average energy E_j^{av} of the two $s=\pm\frac{1}{2}$ components of the jth level is obtained by taking the average of Eq. (2) and is given by

$$E_j^{\mathrm{av}}(k_H=0)=[(E_G/2)^2+j\gamma H]^{1/2} . \qquad (12)$$

In the present work we show that Eq. (12) is also applicable to the energy of the jth level in the present tin-doped bismuth sample.

Using values of $\epsilon=8.6$ meV and $\gamma=81.2$ meV^2/kG determined from the least-squares analysis described below, we obtain the calculated results for the $j=1$ level shown with open circles in Fig. 6. It is seen that Eq. (12) for $j=1$, reproduces E_1^{av} for the experimental curve quite well.

Since the energy of the jth level shown in Fig. 6 is deduced on the basis that the energy is a function only of jH, Eq. (12) is applicable for all j quantum numbers, $j \neq 0$. It is concluded, therefore, that the characteristic functional form [Eq. (12)] of the two-band model also describes the magnetic field dependence of the bands in the present sample of tin-doped bismuth.

In Fig. 7(b) which shows the splitting of the valence- and conduction-band $j = 0$ levels, the field dependence is linearly extrapolated to zero field so as to coincide with $E_G = 2\epsilon$ the energy gap at zero field. It is to be noted that the Fermi level estimated in Sec. II lies below the $j = 0$ levels throughout the magnetic field range of the present investigation, so that the $j = 0$ levels can serve as final states for the Landau-level transitions. The results of the analysis for the A, B, C, and D transitions shown in Fig. 7(b) indicate that, as in the case for pure bismuth, the separation of the $j = 0$ levels decreases with increasing magnetic field until a minimum energy separation $2\delta H_0$ is reached[18] at a magnetic field $H_0 = \epsilon/\alpha'$.

VI. RIGID-BAND MODEL

With the assignments given in Sec. V the gap energy and the four magnetic field coefficients are determined using a least-squares analysis, in which data for the $4 \leftrightarrow 5$ and the $5 \leftrightarrow 6$ transitions above 120 meV together with all the data for the $1 \leftrightarrow 2$, $2 \leftrightarrow 3$, $3 \leftrightarrow 4$, and $0 \leftarrow 1$; A, B, C, and D transitions are treated with the same weight and fitted to transition energies derived from Eqs. (2), (6), and (9). The values obtained are compared with those of pure bismuth in Table I. The results show that

there is little difference between the tin-doped bismuth and pure bismuth with regard to the momentum matrix element γ between the conduction and valence bands and the splitting factor α for the $j \neq 0$ levels. In this connection it should be noted that the momentum matrix element of bismuth also is almost invariant under variation of the temperature, pressure, and antimony concentration (up to at least 10 at. % Sb). However, the gap energy E_G is approximately 1.25 times as large as that of pure bismuth, and the field coefficients α' and δ associated with the $j = 0$ level are also large in comparison with those of pure bismuth. Since E_G for bismuth is very small, the magnitude of the change in E_G for the tin-doped sample relative to that in pure bismuth is still a small energy. The energy gap has also been found to exhibit large relative changes upon variation of temperature,[19] pressure,[20] and the addition of antimony.[12]

It is concluded, therefore, that the basic form of the electronic energy-level scheme is maintained upon doping with tin. The fact that the momentum matrix element γ is nearly the same as that of pure bismuth indicates that the band-edge wave functions of the conduction and valence bands remain essentially unperturbed by the doping. The same conclusion that the band-edge wave functions remain unchanged also follows from the observation that the splitting factor α shows no appreciable change, because α comes from the $\vec{k} \cdot \vec{p}$ perturbation due to bands other than the conduction and valence bands of the two-band model,[18,23] and the energies and wave functions of those other bands are not expected to change very much with such a small density of tin impurities.

The results show that the effects of the tin dop-

TABLE I. A comparison of band parameters of tin-doped bismuth with those of pure bismuth.

Parameters[a]	Units	Tin-doped bismuth[b]	Pure bismuth[c]
ϵ	meV	8.6 ± 0.1	6.9
γ	meV^2/kG	81.2 ± 0.1	82.1
α	meV/kG	0.043 ± 0.002	0.045
α'	meV/kG	0.083 ± 0.007	0.067
δ	meV/kG	0.066 ± 0.002	0.015

[a]The parameters in the table are defined by: $\epsilon \equiv E_G/2$, $\gamma \equiv E_G \beta^*$, $\alpha \equiv G\beta^*$, $\alpha' \equiv |G_0\beta^*|$, and $\delta \equiv P\beta^*$.

[b]The tin-doped bismuth sample in the present investigation has an excess-hole concentration of $\Delta = 4.28 \times 10^{18}$ cm^{-3}.

[c]Data from Ref. 18.

ing are essentially confined to the vicinity of the band gap, which is increased by the tin doping. The field coefficient δ in Eq. (6) represents the effect of bands outside the strict two-band model[18,23] and connects levels of bands with different parities L_s and L_a, i.e., δ is a matrix element between the $j = 0$ levels in the valence and conduction bands. As is discussed further in Sec. VII impurity doping introduces this type of perturbation which effectively breaks the inversion symmetry of the lattice in the vicinity of the impurity site, because a localized impurity can absorb crystal momentum. The values of α' in Eq. (6) increase in comparison with that of pure bismuth, while the magnetic field of minimum separation $H_0 = \epsilon/\alpha'$ is almost the same as that of pure bismuth. Besides α, which is unchanged from that of pure bismuth as is described above, the coefficient α' includes a term which arises via second-order $\vec{k} \cdot \vec{p}$ perturbation theory from the bands other than the strongly coupled conduction and valence bands at the L point, and is evaluated from analysis of transitions between the four $j = 1$ levels and the two $j = 0$ levels.[18] This term is proportional to ϵ due to the difference in contributions from the $j = 1$ levels in the conduction band and those in the valence band,[18] and the observed result indicates that this term also contributes to the determination of α' for the tin-doped bismuth sample.

It is of interest to note that the band gap in bismuth increases upon application of pressure,[20] suggesting that the addition of tin to bismuth might introduce stress to the lattice. According to Mott and Jones[30] the energy gap at the L point of bismuth is related to the total electron energy which is decreased with increasing density of acceptor impurities in the present tin-doped bismuth sample and might result in a decrease in the internal displacement of the bismuth lattice. In 0.125 at. % tin-doped bismuth no changes in the lattice constants and little decrease in the internal displacement are observed in comparison with those of pure bismuth.[31] It would be interesting to investigate the value of the internal displacement and that of the energy gap as a function of the tin acceptor concentration.

Shubnikov—de Haas (SdH) measurements performed on tin-doped bismuth samples of comparable impurity concentrations are reported in Ref. 7. These experiments give no evidence of any shift of the L_s conduction and L_a valence bands with respect to each other. On the other hand, the magnetoreflection experiment is much more sensitive to

these shifts than are the SdH measurements. Bate and co-workers[7] did perhaps find a slight upshift of L_a with respect to the T-hole band, but this effect, in turn, cannot be seen in the present results.

The SdH measurements also are inconsistent with the hypothesis that L_a and L_s are "mirror bands."[7] Through a study of the anisotropy of the SdH periods in Ref. 7 these authors concluded that for the field in the trigonal direction, the longitudinal effective mass in the L_a band is not more than $\frac{1}{3}$ that in the L_s band.

With regard to the magnetoreflection experiment for the field along a binary direction, there is no evidence for any departure from mirror-band behavior. Another conclusion in Ref. 7 on samples of comparable doping concentration is that the T-point holes still remain in a spheroidal Fermi surface, but that the ratio of the major to the minor axis of this spheroid is slightly reduced ($\sim 1\%$ for a Sn concentration of 4×10^{18} cm^{-3}) with respect to that in pure bismuth. This conclusion has essentially no effect on the analysis of the L-point transitions presented here.

VII. IDENTIFICATION OF OTHER LINES

From the splittings given in Figs. 7(a) and 7(b) together with the level energies shown in Fig. 6, the field dependence of all possible transitions which are forbidden in pure bismuth can be deduced. From this analysis it is found that the satellites s_j of the $j \leftrightarrow j + 1$ transitions are identified with a superposition of the forbidden $j \rightarrow j$ and $j - 1 \leftrightarrow j + 1$ transitions, i.e., those for $\Delta j = 0$ and ± 2. In Fig. 8 the possible transitions (lines) are compared with the experimental results (points) and the s_j transitions are thereby identified. For example, in the case of the s_3 satellite, the satellite of the $3 \leftrightarrow 4$ transitions, the calculated locations of the $3 \leftrightarrow 3$ and $2 \leftrightarrow 4$ transitions are very close to each other and the observed points fall nicely between those calculated for the above two transitions.

Among the two transitions that contribute to a given satellite, the $\Delta j = \pm 2$ transitions are located at higher magnetic fields than the $\Delta j = 0$ transitions, and the difference in resonant field between the two transitions increases with increasing photon energy and with decreasing j quantum number, thus giving rise to a broadening of the line shapes for the s_j transitions. For example, for the s_2 satellite the splitting between the $2 \rightarrow 2$ and $1 \leftrightarrow 3$ transitions is about 2 kG at the photon energy of
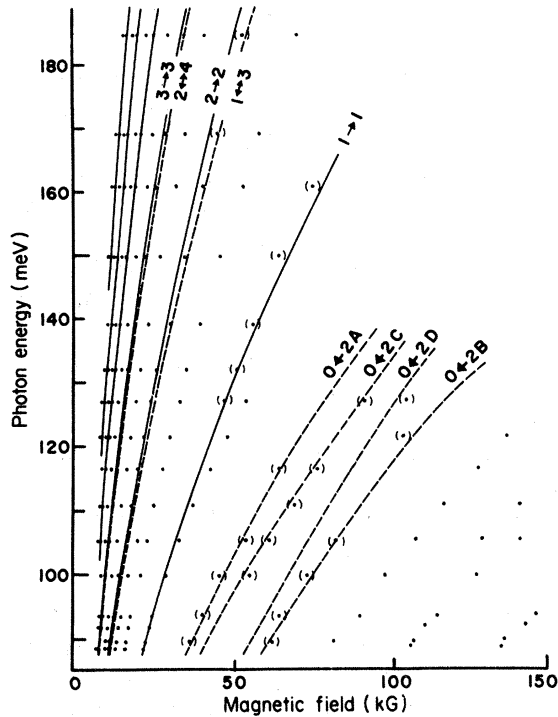
FIG. 8. Assignment of the satellite lines and broad
and weak structures (see Fig. 4). A dot represents the
measured location of a well-defined resonance and a dot
in parenthesis shows the approximate location of a
broad and weak structure. The solid and dashed lines
represent the location of the $\Delta j = 0$ and $\Delta j = \pm 2$ transi-
tions, respectively, calculated from level energies shown
in Figs. 6 and 7. All transitions identified in this figure
are forbidden in pure bismuth.

150 meV. At this photon energy a noticeable
broadening of the s_2 satellite line shape is observed.

The location of the $1 \leftrightarrow 4$ transition is calculated
to be about halfway between the $2 \leftrightarrow 3$ main transi-
tion and the s_2 satellite. Also, the $1 \leftrightarrow 5$ transition
is expected to be located between the s_3 satellite
and the $2 \leftrightarrow 3$ main transition. No structure is ob-
served at these locations and it is therefore inferred
that the $|\Delta j| \geq 3$ transitions have low intensities.

We attribute the breakdown in the selection rules
for pure bismuth to the presence of tin impurities.
Within the category of spin-conserving transitions,
the $\Delta j = 0$ and $\Delta j = \pm 2$ selection rules imply
$\Delta n = \pm 1$ for the selection rules on the orbital
Landau-level quantum number. These transitions
correspond to and usually are the strongest of
those that obey the general selection rule
$\Delta n = \pm (2l + 1)$. Such $\Delta n = \pm (2l + 1)$ transitions

take place in a lattice with no inversion symmetry.
In such a lattice the crystal momentum component
(perpendicular to the magnetic field) of the
conduction-band minimum is displaced from that
of the valence-band maximum. Since the lattice of
the present sample of tin-doped bismuth essentially
retains its inversion symmetry, the observed $\Delta j = 0$
or $\Delta j = \pm 2$ transitions are assigned to indirect
transitions between Landau levels of two nonprin-
cipal L points, i.e., from the jth level near one L
point to the jth or $(j \pm 2)$th level near the other L
point and vice versa, so that the difference in crys-
tal momentum between the initial and final levels
is absorbed by a localized impurity. Note that the
Landau levels associated with each L point are
similar to the corresponding levels in pure bismuth.

We observe no transitions that violate the spin-
selection rule for transitions which do not involve
the $j = 0$ levels. Thus, there is no change in the
selection rule for Δs, which remains $\Delta s = \pm 1$. All
faint and broad structures which are shown in Fig.
4 with dots in parentheses are located in the mag-
netic field range between the a_2 line and the $0 \leftarrow 1$;
A, C, D, and B transitions, and can be identified
with one of the $0 \leftarrow 2$; A, C, D, and B transitions, as
shown in Fig. 8.

The s_1 satellite which is located on the high-
magnetic-field side of the $1 \leftrightarrow 2$ transition and the
high-photon-energy side of the a_1 line is different
from the other satellite transitions and is not la-
beled in Figs. 3 and 4 due to the weakness of the
structure. This satellite line consists of a single
$1 \rightarrow 1$ transition, contrary to the other satellite lines
which consist of both the $\Delta j = 0$ and $\Delta j = \pm 2$ tran-
sitions. As is shown in Fig. 8, the locations of the
$0 \leftarrow 2$ transitions are calculated to be in the region
of higher magnetic fields and not near the s_1 line.
Although the s_1 satellite is identified with a single
transition, the observed structure is broad at all the
photon energies that were investigated in this
work. Furthermore, its intensity is very weak,
weaker than what might be expected, even taking
into account that it is a single transition. It should
be noted that the expected location of the $1 \rightarrow 1$
transition moves closer to the observed a_1 line with
decreasing photon energy and almost coincides
with it below a photon energy of about 100 meV
where the a_1 line is intense and sharp.

Except for this coincidence the additional a_1 and
a_2 lines cannot be identified with any transitions
between the Landau levels within the scheme given
in Figs. 6 and 7, which is qualitatively similar to
that of pure bismuth. Several transitions have
been examined in order to identify the a_1 and a_2

additional lines, including transitions within the level scheme described above, transitions between impurity levels with a Fermi-level cutoff, and impurity-enhanced indirect transitions from Landau levels associated with the nonprincipal L points to those associated with the principal L point and to those associated with the T point. All these attempts were found to be unsatisfactory in explaining the observed field dependence of the a_1 and a_2 lines.

We further note that the intensities of the a_1 and a_2 transitions are too strong to assign them to transitions between levels of an impurity of such a small concentration. No splittings of the a_1 and a_2 transitions are observed in the recorder traces. We also note that the field dependences of the a_1 and a_2 transitions are curved similarly to those between the bismuth-type Landau levels, although the a_j ($j \geq 3$) transitions are not observed experimentally, probably due to a superposition of other transitions.

Therefore the a_1 and a_2 lines are tentatively assigned to transitions between the impurity-perturbed Landau levels, namely, between the Landau levels of the cyclotron motions of electrons under an impurity potential described by a linear combination of wave functions for the two nonprincipal L points. At the magnetic fields where the a_1 and a_2 transitions disappear (see Fig. 4), the radii of the $n = 1$ and $n = 2$ cyclotron orbits in a parabolic band are 200 and 400 Å, respectively. For higher magnetic fields the radii become smaller so that the electrons no longer have an impurity within their orbits, since the average separation between the impurities is estimated to be ~80 Å in the present sample of tin-doped bismuth. At these higher magnetic fields the electrons revert back to normal cyclotron motion similar to that in pure bismuth and the impurity-perturbed transitions disappear.

The field dependence of the a_1 and a_2 lines are fitted to the transition energies derived from Eqs. (6) and (12), based on the assumptions that the impurity-perturbed Landau levels are of the bismuth type, and that the a_1 and a_2 lines are the 1↔2 and 2↔3 transitions, respectively. The values of parameters thus determined are $\epsilon = 24$ meV and $\gamma = 44$ meV^2/kG, and are different from those for the nonperturbed magnetic levels listed in Table I. The fitting is only approximate because the

discrepancy between the observed and assumed field dependence slightly exceeds the experimental error. On the other hand, the large difference in γ for pristine and doped bismuth is attributed to the potential of charged impurities $-e/\kappa r$, where κ is the high-frequency dielectric constant; in this connection the expectation value of $1/r$ in a Landau level is proportional to $\sqrt{H}$, which properly describes the field dependence. By equating the energy associated with the difference in γ to that of the impurity potential, we obtain $\kappa = 1.2$, a reasonable value for the dielectric constant. The result of this evaluation supports the present assignment of the a_1 and a_2 lines.

Although bismuth-type levels are used in the present analysis, there is no experimental evidence that the impurity-perturbed Landau levels are the mirror image of each other. Since acceptors mainly perturb the valence band, the levels associated with the additional lines might possibly be related to the Fermi-surface cross sections found by Bate and co-workers in their SdH measurements.[7]

In order to clarify the properties of the impurity-perturbed Landau levels, it is necessary to extend the magnetoreflection measurements to the lower-photon-energy region and accurately determine the field dependence of these additional transitions.

In conclusion, we have observed additional a_1 and a_2 transitions and have tentatively assigned them to transitions between impurity-perturbed Landau levels. It is further emphasized that these impurity-perturbed Landau levels are different from the magnetic levels of the rigid-band model.

ACKNOWLEDGMENTS

*Visitor, Francis Bitter National Magnet Laboratory, supported by National Science Foundation.

[1]N. B. Brandt and M. V. Razumeenko, Zh. Eks. Teor. Phys. 39, 276 (1960) [Sov. Phys.—JETP 12, 198 (1961)].

[2]H. Jones, Proc. R. Soc. London, Sect. A 147, 396 (1934).

[3]N. Thomson, Proc. R. Soc. London, Ser. A 155, 111 (1936).

[4]D. Shoenberg and M. Z. Uddin, Proc. R. Soc. London, Ser. A 156, 687 (1936); 156, 701 (1936).

[5]J. M. Noothoven van Goor, Philips Res. Rep. Suppl. 4 (1971).

[6]R. T. Bate and N. G. Einspruch, Phys. Rev. 153, 796 (1967).

[7]R. T. Bate, N. G. Einspruch, and P. J. May, Phys. Rev. 186, 599 (1969).

[8]R. T. Bate, W. R. Mardin, and N. G. Einspruch, J. Appl. Phys. 38, 4852 (1967).

[9]G. A. Antcliffe and R. T. Bate, Phys. Rev. 160, 531 (1967).

[10]A. L. Jain, Phys. Rev. 114, 1518 (1959).

[11]F. A. Buot, in Proceedings of the International Conference on the Physics of Semimetals and Narrow-Gap Semiconductors, Dallas, Texas, 1970, edited by D. L. Carter and R. T. Bate (Pergamon, New York, 1971), p. 99.

[12]E. J. Tichovolsky and J. G. Mavroides, Solid State Commun. 7, 927 (1969).

[13]J. Heremans, Ph.D. thesis, Louvain-la-Neuve, 1979 (unpublished).

[14]O. P. Hansen and J. Heremans, Recent Developments in Condensed Matter Physics, edited by J. T. Devreese et al. (Plenum, New York, 1981), Vol. 3, p. 1.

[15]R. N. Brown, J. G. Mavroides, and B. Lax, Phys. Rev. 129, 2055 (1963).

[16]M. Maltz and M. S. Dresselhaus, Phys. Rev. B 2, 2877 (1970).

[17]M. P. Vecchi and M. S. Dresselhaus, Phys. Rev. B 9, 3257 (1974).

[18]M. P. Vecchi, J. R. Pereira, and M. S. Dresselhaus, Phys. Rev. B 14, 298 (1976).

[19]M. P. Vecchi and M. S. Dresselhaus, Phys. Rev. B 10, 771 (1974).

[20]E. E. Mendez, A. Misu, and M. S. Dresselhaus, Phys. Rev. B 24, 639 (1981).

[21]M. H. Cohen and E. I. Blount, Philos. Mag. 5, 115 (1960).

[22]P. A. Wolff, J. Phys. Chem. Solids 25, 1067 (1964).

[23]G. A. Baraff, Phys. Rev. 137, A842 (1965).

[24]J. E. Smith, G. A. Baraff, and J. M. Rowell, Phys. Rev. 135, A1118 (1964).

[25]V. S. Edelman and M. S. Khaikin, Zh. Eksp. Teor. Phys. 49, 107 (1965) [Sov. Phys.—JETP 22, 77 (1966)].

[26]R. N. Bhargara, Phys. Rev. 156, 785 (1967).

[27]M. S. Dresselhaus, in Proceedings of the International Conference on the Physics of Semimetals and Narrow Gap Semiconductors, Dallas, Texas, 1970, edited by D. L. Carter and R. T. Bate (Pergamon, New York, 1971), p. 3.

[28]J. Boxus, J. Heremans, J.-P. Michenaud, and J.-P. Issi (unpublished).

[29]J. Heremans, J. Boxus, and J.-P. Issi (unpublished).

[30]N. F. Mott and H. Jones, The Theory of the Properties of Metals and Alloys (Clarendon, Oxford, 1936), p. 166.

[31]P. Cucka and C. S. Barrett, Acta Crystallogr. 15, 865 (1962).